

# In Vitro Assembly as a Tool to Investigate Catalytic Intermediates of [NiFe]-Hydrogenase

Giorgio Caserta,\* Christian Lorent, Vladimir Pelmeshnikov, Janna Schoknecht, Yoshitaka Yoda, Peter Hildebrandt, Stephen P. Cramer, Ingo Zebger,\* and Oliver Lenz\*



Cite This: *ACS Catal.* 2020, 10, 13890–13894



Read Online

ACCESS |

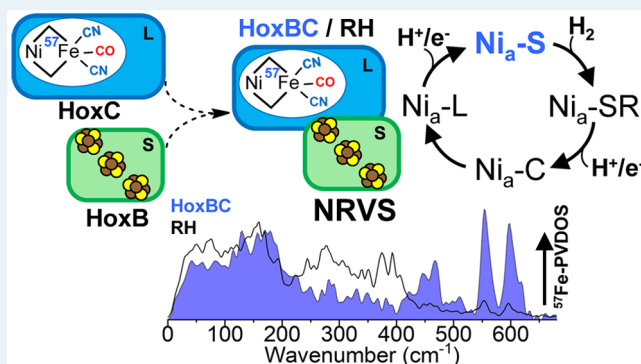
Metrics & More

Article Recommendations

Supporting Information

**ABSTRACT:** [NiFe]-hydrogenases catalyze the reversible reaction  $\text{H}_2 \rightleftharpoons 2\text{H}^+ + 2\text{e}^-$ . Their basic module consists of a large subunit, coordinating the NiFe(CO)(CN)<sub>2</sub> center, and a small subunit that carries electron-transferring iron–sulfur clusters. Here, we report the *in vitro* assembly of fully functional [NiFe]-hydrogenase starting from the isolated large and small subunits. Activity assays complemented by spectroscopic measurements revealed a native-like hydrogenase. This approach was used to label exclusively the NiFe(CO)(CN)<sub>2</sub> center with <sup>57</sup>Fe, enabling a clear view of the catalytic site by means of nuclear resonance vibrational spectroscopy. This strategy paves the way for in-depth studies of [NiFe]-hydrogenase catalytic intermediates.

**KEYWORDS:** metalloenzyme, hydrogenase, hydrogen, nickel, iron, catalytic cycle, spectroscopy



Utilizing the naturally abundant nickel and iron, [NiFe]-hydrogenases catalyze the reversible interconversion of  $\text{H}_2$  into protons and electrons close to the thermodynamic potential and at high turnover frequencies.<sup>1,2</sup> [NiFe]-hydrogenases are multisubunit enzymes that generally contain a heterodimeric hydrogenase module composed of a large subunit harboring the catalytic NiFe(CO)(CN)<sub>2</sub> center and a small subunit equipped with iron–sulfur clusters.<sup>3,4</sup> The O<sub>2</sub>-tolerant regulatory [NiFe]-hydrogenase (RH) from *Ralstonia eutropha* represents a valuable model enzyme characterized in detail using a variety of spectroscopic techniques.<sup>5–7</sup> One key advantage is that the RH active site can be enriched in two intermediate states of the catalytic cycle (i.e., Ni<sub>a</sub>-S and Ni<sub>a</sub>-C). In the Ni<sub>a</sub>-S state, the bridging position between the Ni and Fe ions remains vacant, while the Ni<sub>a</sub>-C state is characterized by a bridging hydride (Figure 1). We have shown recently that the RH large subunit HoxC—when detached from the small subunit HoxB—exhibits catalytic and spectroscopic properties that are quite different from those of native RH.<sup>5,8</sup> Therefore, the question arose of whether the isolated HoxC subunit would interact with the small subunit HoxB to produce a fully functional [NiFe]-hydrogenase. Here, we addressed this problem by reporting the *in vitro* reconstitution of a [NiFe]-hydrogenase based on the independent purification of the two subunits and their subsequent assembly.

The RH large subunit HoxC was purified as described before (Supporting Information).<sup>8</sup> Consistent with previous infrared (IR) spectroscopic investigations, the as-isolated HoxC protein (HoxC<sub>ai</sub>) contains an intact active site residing

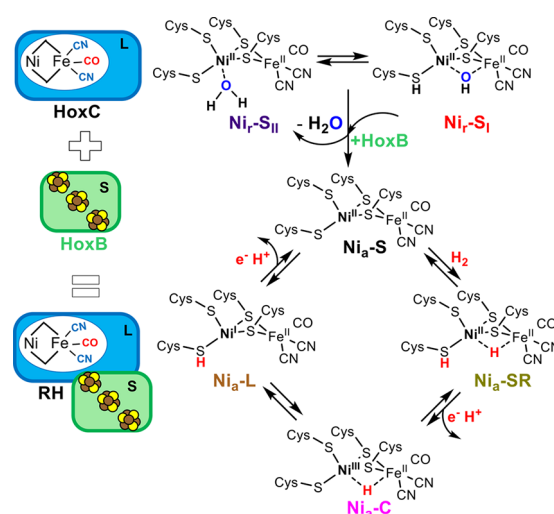


**Figure 1.** *In vitro* assembly of the regulatory [NiFe]-hydrogenase. The isolated large subunit, HoxC (blue, L), resides in the Ni<sub>a</sub>-S<sub>I</sub> and Ni<sub>a</sub>-S<sub>II</sub> resting states. Upon addition of the small subunit HoxB (green, S), the HoxBC complex is formed, which possesses the typical catalytic intermediates Ni<sub>a</sub>-S, Ni<sub>a</sub>-SR, Ni<sub>a</sub>-C, and Ni<sub>a</sub>-L. See text for details.

Received: September 17, 2020

Revised: November 5, 2020

predominantly in the diamagnetic resting states  $\text{Ni}_I\text{-S}_{\text{II}}$  and  $\text{Ni}_I\text{-S}_{\text{II}}$  (Figure 2). These states are supposed to harbor water-derived ligands at the active site (Figure 1).<sup>8</sup> By contrast, as-isolated RH ( $\text{RH}_{\text{ai}}$ ) resided predominantly in the  $\text{Ni}_I\text{-S}$  state (Figure 2). Upon incubation of  $\text{RH}_{\text{ai}}$  with  $\text{H}_2$ , the  $\text{Ni}_I\text{-C}$  state was enriched.<sup>5,9,10</sup> Previous experiments on  $\text{HoxC}_{\text{ai}}$  revealed that the same  $\text{H}_2$  treatment did not cause any change of the active site.<sup>8</sup> Contrary to  $\text{HoxC}$ , the  $\text{HoxB}$  subunit was aerobically purified as N-terminally Strep-tagged protein from the heterologous host *Escherichia coli* (Supporting Information, Figures S1–S3, Table S1). Previous EPR and Mössbauer studies on native RH indicated that  $\text{HoxB}$  harbors three  $[\text{4Fe-4S}]$  clusters with different midpoint potentials.<sup>5</sup>

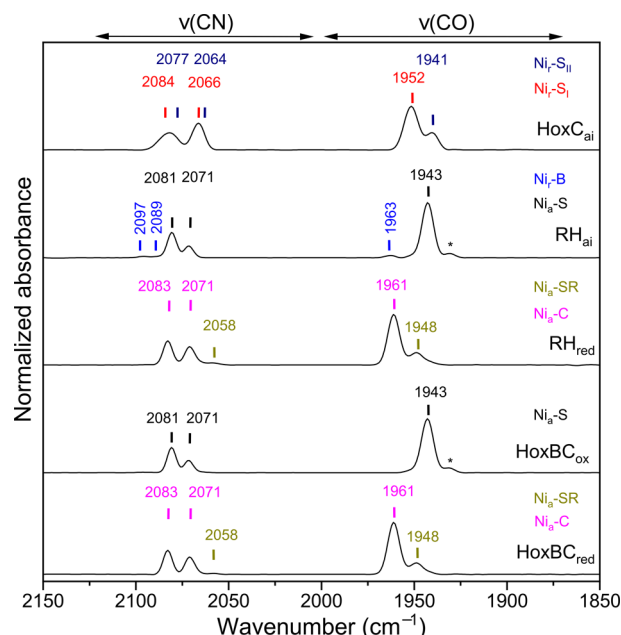


**Figure 2.** Infrared spectra of as-isolated  $\text{HoxC}$  ( $\text{HoxC}_{\text{ai}}$ ), as-isolated RH ( $\text{RH}_{\text{ai}}$ ),  $\text{H}_2$ -reduced RH ( $\text{RH}_{\text{red}}$ ), oxidized  $\text{HoxBC}$  complex ( $\text{HoxBC}_{\text{ox}}$ ), and  $\text{H}_2$ -reduced  $\text{HoxBC}$  complex ( $\text{HoxBC}_{\text{red}}$ ). The redox state-sensitive positions of the IR bands are related to the stretching vibrations of the CO and CN ligands of the  $[\text{NiFe}]$ -hydrogenase active site. The color code for the band labels is as defined in Figure 1. The bands marked with an asterisk refer presumably to minor amounts of  $\text{Ni}_I\text{-S}$  species. The IR spectra of RH and the  $\text{HoxBC}$  complex are normalized with respect to the dominant CO absorption.

To characterize the Fe–S clusters of freshly purified, as-isolated  $\text{HoxB}$  ( $\text{HoxB}_{\text{ai}}$ ), we performed continuous-wave (cw) X-band EPR spectroscopy.  $\text{HoxB}_{\text{ai}}$  appeared to be mainly EPR-silent with trace signals of  $[\text{3Fe-4S}]^+$  clusters, consistent with partial  $[\text{4Fe-4S}]$  cluster degradation (Figure 3a, Figure S4a).<sup>5</sup> Notably, minor  $[\text{3Fe-4S}]^+$  species were detected also in native RH (Figure S4b). Reduction of  $\text{HoxB}_{\text{ai}}$  with sodium dithionite produced a rhombic EPR signal ascribed to a reduced  $[\text{4Fe-4S}]^+$  cluster (Figure S4a, Table S2).

Further power- and temperature-dependent EPR measurements indicated additional minor signals of the  $[\text{4Fe-4S}]$  clusters (Figure S4c,d). The partial reduction of the iron–sulfur cluster relay in  $\text{HoxB}$  is in line with previous observations for native RH.<sup>5</sup>

For *in vitro* assembly of  $\text{HoxBC}$ ,  $\text{HoxC}_{\text{ai}}$ , and  $\text{HoxB}_{\text{ai}}$  were incubated for 2 h in different ratios at pH 8.0 and 10 °C under anoxic conditions in the presence of a 10–15-fold molar excess

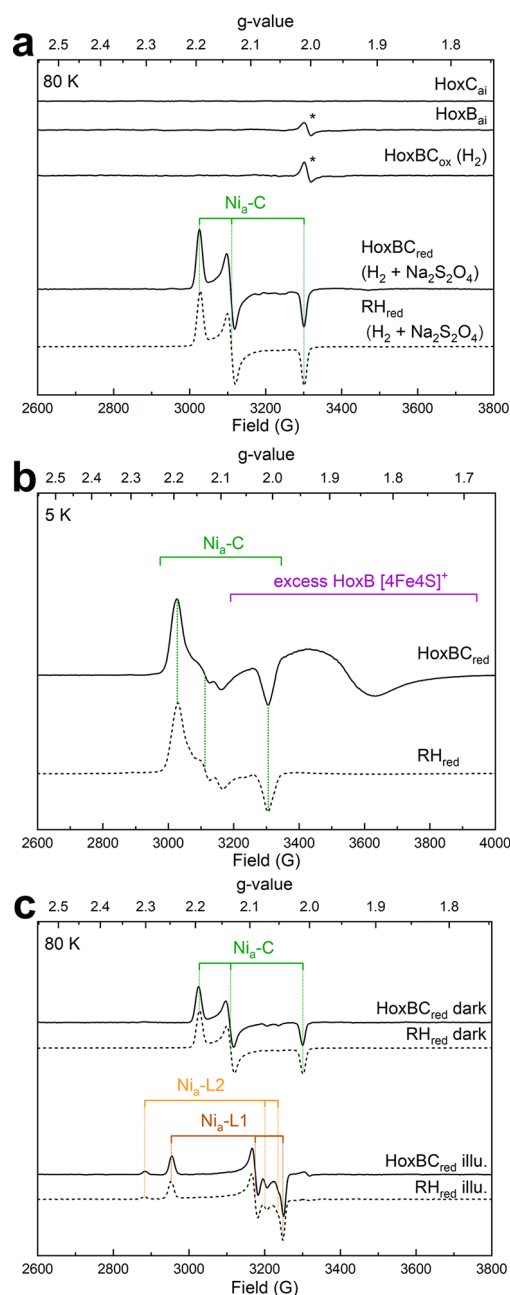


**Figure 3.** EPR spectra of native RH,  $\text{HoxB}_{\text{ai}}$ ,  $\text{HoxC}_{\text{ai}}$ , and the  $\text{HoxBC}$  complex taken under different redox and illumination conditions. (a) From top to bottom: EPR spectra at 80 K of  $\text{HoxC}_{\text{ai}}$ ,  $\text{HoxB}_{\text{ai}}$ , a mixture of  $\text{HoxB}_{\text{ai}}$  and  $\text{HoxC}_{\text{ai}}$  treated with  $\text{H}_2$ , the  $\text{HoxBC}$  mixture treated with sodium dithionite and  $\text{H}_2$ , and likewise treated RH. The g values of the  $\text{Ni}_I\text{-C}$  species (green) are  $g_x = 2.193$ ,  $g_y = 2.135$ , and  $g_z = 2.011$  (Table S2). Minor signals indicated by asterisks are attributable to  $[\text{3Fe-4S}]^+$  clusters of the  $\text{HoxB}$  subunit. (b) EPR spectra of the reduced  $\text{HoxBC}$  complex and native RH recorded at 5 K. The characteristic split and broadened  $\text{Ni}_I\text{-C}$  signal arose from the dipolar and exchange coupling of the paramagnetic  $[\text{NiFe}]$  site and the proximal  $[\text{4Fe-4S}]^+$  cluster. The spectral contributions indicated with a violet bracket are assigned to  $[\text{4Fe-4S}]^+$  clusters of unbound  $\text{HoxB}$ . (c) EPR spectra recorded at 80 K for reduced  $\text{HoxBC}$  complex (solid lines) and native RH (dashed lines) before and after illumination (illu.) with LED light (455 nm). The g values for the light-induced  $\text{Ni}_I\text{-L1}$  and  $\text{Ni}_I\text{-L2}$  signals are  $g_x = 2.248$ ,  $g_y = 2.091$ ,  $g_z = 2.044$  and  $g_x = 2.302$ ,  $g_y = 2.074$ ,  $g_z = 2.051$ , respectively (Table S2). EPR spectra related to native RH as a control are displayed in gray.

of sodium dithionite and a continuous flow of H<sub>2</sub>. A 5-fold excess of HoxB over HoxC, resulted in the highest specific activity of (6.0 ± 0.7) U·mg<sup>-1</sup>, which was measured spectrophotometrically as H<sub>2</sub>-mediated reduction of methylene blue. For comparison, the specific activity of native RH reached values of (4.5 ± 0.3) U·mg<sup>-1</sup>. The 5:1 ratio of HoxB:HoxC that was required for full activity owes to the fact that the HoxB preparation (Figure S3) was less homogenous than that of HoxC. Importantly, the individual HoxC<sub>ai</sub> and HoxB<sub>ai</sub> subunits did not exhibit any activity under these conditions. IR spectroscopic investigation of reconstituted HoxBC revealed the characteristic CO and CN bands attributed to the diatomic ligands of the [NiFe] cofactor, thereby confirming the successful assembly of the two RH subunits (Figure 2). In H<sub>2</sub>-reduced HoxBC, we observed the typical CO and CN bands of the catalytic intermediate Ni<sub>a</sub>-C ( $\nu_{\text{CO}} = 1961 \text{ cm}^{-1}$ ) in addition to minor amounts of Ni<sub>a</sub>-SR ( $\nu_{\text{CO}} = 1948 \text{ cm}^{-1}$ ) (Figure 2, Table S3). Oxidative treatment of reduced HoxBC with air led to the accumulation of the Ni<sub>a</sub>-S state with a characteristic CO band at 1943 cm<sup>-1</sup>, as also observed for as-isolated native RH.

Complementary EPR spectroscopic studies revealed the typical signature of the paramagnetic Ni<sub>a</sub>-C state in the reduced HoxBC complex (Figure 3a). Notably, the corresponding g-values are basically identical to those obtained for reduced native RH (Table S2).<sup>11</sup> Lowering the temperature to 5 K led to the broadening and partial splitting of the Ni<sub>a</sub>-C signal, indicative for the magnetic interaction between the paramagnetic [NiFe] active site and the reduced proximal [4Fe-4S]<sup>+</sup> cluster. The same split signal was observed for native RH (Figure 3b).<sup>5</sup> Importantly, neither HoxB<sub>ai</sub> or HoxC<sub>ai</sub> nor a mixture of both proteins incubated with H<sub>2</sub> showed any relevant EPR signal (Figure 3a). This indicates that reduction of HoxB is a prerequisite for HoxBC dimer assembly and subsequent formation of the Ni<sub>a</sub>-C state. In standard [NiFe]-hydrogenases, illumination at cryogenic temperatures converts the Ni<sub>a</sub>-C state into the Ni<sub>a</sub>-L state, which is suggested to be an intermediate of the catalytic cycle.<sup>12–14</sup> Thus, we investigated the light sensitivity of the Ni<sub>a</sub>-C state in HoxBC. A reduced sample was first flash-frozen in the dark and the Ni<sub>a</sub>-C state monitored by EPR spectroscopy (Figure 3c). Subsequently, the sample was illuminated with LED light (455 nm) at 80 K, which resulted in the Ni<sub>a</sub>-C-to-Ni<sub>a</sub>-L conversion, identical to the behavior of native RH (Figure 3c). In fact, we detected two different Ni<sub>a</sub>-L species, designated Ni<sub>a</sub>-L1 and Ni<sub>a</sub>-L2 (Table S2), whose structural difference is still under debate.<sup>15–17</sup>

The *in vitro* assembly of the RH allows an unprecedented spectroscopic view onto the catalytic center of mature [NiFe]-hydrogenases. The independent purification of the two subunits and their subsequent assembly enables specific labeling of either of the subunits with, for example, <sup>57</sup>Fe, which can be exploited by applying isotope-sensitive techniques such as nuclear resonance vibrational spectroscopy (NRVS). In case [NiFe]-hydrogenases have been uniformly labeled with <sup>57</sup>Fe, vibrational bands of the catalytic center are detectable exclusively in the 420–630 cm<sup>-1</sup> region. Active-site-related signals in the low-frequency region (0–420 cm<sup>-1</sup>) are usually obscured by the strong Fe–S cluster signals.<sup>18–20</sup>

To suppress the Fe–S cluster signals, we generated a HoxBC complex where only the HoxC subunit was enriched with <sup>57</sup>Fe. Figure 4a shows the NRVS spectra of uniformly labeled RH and site-specifically labeled HoxBC, both enriched in the Ni<sub>a</sub>-S state. Active-site labeling of the HoxBC protein led to a relative

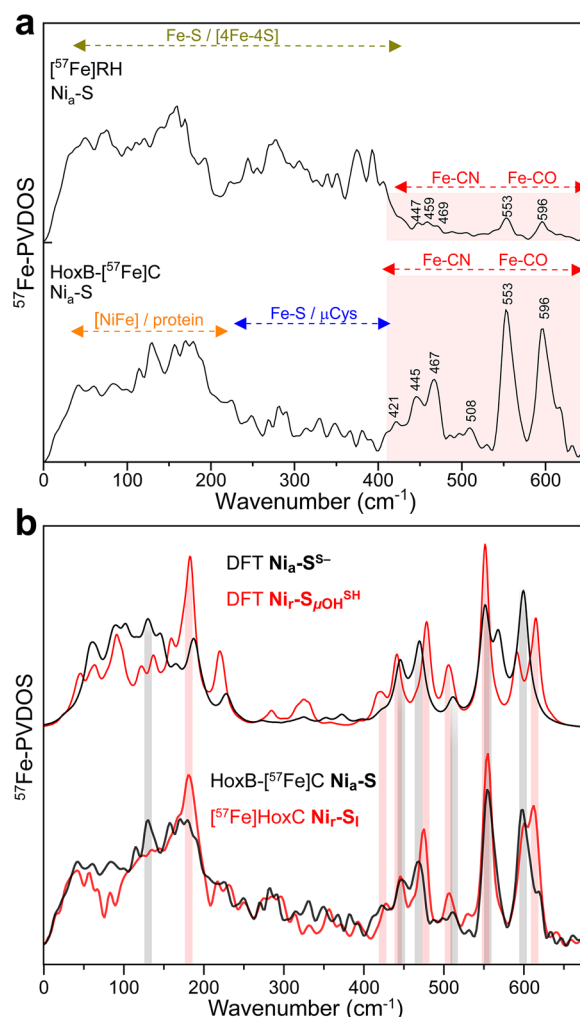


**Figure 4.** NRVS of reconstituted and selectively labeled HoxBC in comparison to native RH. (a) <sup>57</sup>Fe-PVDOS data of the assembled HoxB-[<sup>57</sup>Fe]C complex and native [<sup>57</sup>Fe]RH, both enriched in the Ni<sub>a</sub>-S state. (b) <sup>57</sup>Fe-PVDOS data of the HoxB-[<sup>57</sup>Fe]C complex (black trace) and [<sup>57</sup>Fe]HoxC (red trace), along with the corresponding DFT-calculated spectra based on the Ni<sub>a</sub>-S<sup>2-</sup> (black trace) and Ni<sub>a</sub>-S<sub>μOH</sub><sup>SH</sup> (red trace) models (see SI for details). The spectra of [<sup>57</sup>Fe]RH and [<sup>57</sup>Fe]HoxC are adapted from ref 20. The spectral regions in (a) are marked with dashed arrows using the following color code: red, Fe–CO/CN bands of the active site; olive green, Fe–S modes of the [4Fe-4S] clusters; orange, [NiFe]/protein modes; blue, Fe–S modes involving bridging cysteines. Dominant active-site bands in (a) are labeled with the corresponding wavenumbers. Spectra including error bars are shown in Figure S12. In (b), the matching NRVS/DFT bands for Ni<sub>a</sub>-S and Ni<sub>a</sub>-S<sub>1</sub> spectral changes are highlighted by vertical black and red bars, respectively.

increase in intensity of the Fe–CO/CN related bands in the ~400–620 cm<sup>-1</sup> region (Figure 4a, semitransparent red). The dominant bands at 554 and 597 cm<sup>-1</sup> in HoxBC perfectly coincide with those of native RH. Moreover, we also detected active-site-related features in the low-frequency region, which are usually covered by Fe–S cluster modes. By normalizing the spectra to the integral intensities of the main Fe–CO bands, the relatively minor spectral contribution of the [NiFe] active site to the whole NRVS spectrum of RH becomes readily visible (Figure S5). Notably, the selective labeling enabled the observation of mixed Fe–CO/CN bands at 421, 445, 467, and

508  $\text{cm}^{-1}$ , which are hardly resolved in the spectrum of native RH.<sup>20</sup>

DFT calculations performed on a model of HoxBC in the  $\text{Ni}_a\text{-S}$  state successfully reproduced the experimental NRVS data (Figure 4b), as described in detail in the SI (Supporting Results, Figures S6–S10). Notably, our  $\text{Ni}_a\text{-S}^{\text{S}^-}$  active-site model, featuring a vacant substrate binding site between Ni and Fe as well as a deprotonated Ni-bound cysteine Cys479, aligns well with the active-site structure of the  $\text{F}_{420}$ -reducing [NiFe]-hydrogenase from *Methanosarcina barkeri* in the  $\text{Ni}_a\text{-S}$  state (Figure 5).<sup>10</sup> The resolution of the latter was, however,

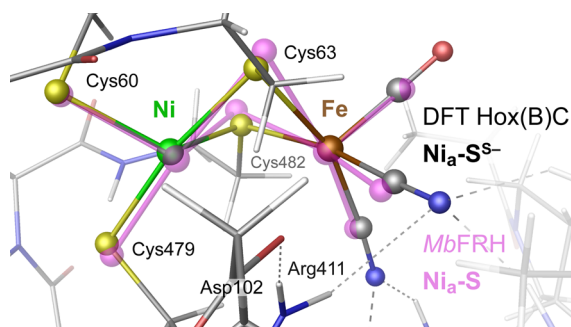


**Figure 5.** DFT model of the RH/HoxBC [NiFe] cofactor in the  $\text{Ni}_a\text{-S}$  state. The metal–ligand core of the  $\text{Ni}_a\text{-S}^{\text{S}^-}$  model (element colors) is superimposed with the X-ray structure of the  $\text{F}_{420}$ -reducing [NiFe]-hydrogenase from *Methanosarcina barkeri* (MbFRH) residing in the  $\text{Ni}_a\text{-S}$  state (semitransparent purple),<sup>10</sup> yielding an RMSD = 0.23 Å for the matching atoms pairs. See Figures S6–S8 for alternative  $\text{Ni}_a\text{-S}$  models and a full-size view of the employed HoxBC homology model.

not high enough to address the protonation state of the corresponding cysteine residue (see SI). The transition from  $\text{Ni}_i\text{-S}$  to the  $\text{Ni}_a\text{-S}$  state involves removal of the metal-bridging hydroxy ligand (Figure 1), which is reflected by complex perturbations of the Fe–CO/CN spectral pattern in the  $\sim 400\text{--}620\text{ cm}^{-1}$  region, and in the  $\sim 100\text{--}200\text{ cm}^{-1}$  region containing [NiFe] cofactor “breathing” modes (Figure 4b).<sup>20</sup> These spectral changes allowed to resolve the two diamagnetic  $\text{Ni}_i\text{-S}$  and  $\text{Ni}_a\text{-S}$  states, which share the same  $\text{Ni}^{\text{II}}\text{Fe}^{\text{II}}$  oxidation level (Figure 1).

The results presented here clearly demonstrate that individually purified [NiFe]-hydrogenase subunits can be assembled *in vitro*, revealing a fully active enzyme. The HoxBC complex formation results in the removal of the water-derived active-site ligands, as demonstrated by the conversion of the  $\text{Ni}_i\text{-S}_{\text{I/II}}$  states dominating in HoxC<sub>ai</sub> into the catalytic intermediates  $\text{Ni}_a\text{-S}$ ,  $\text{Ni}_a\text{-C}$ , and  $\text{Ni}_a\text{-SR}$  states in assembled HoxBC. Furthermore, EPR-based evidence for  $\text{Ni}_a\text{-C}/\text{Ni}_a\text{-L}$  and the magnetic interaction of the paramagnetic active site with the proximal  $[4\text{Fe-4S}]^+$  cluster confirm that the assembled HoxBC complex is identical to native RH. Our strategy paves new avenues to study catalytically relevant [NiFe]-hydrogenase intermediates using <sup>57</sup>Fe-sensitive spectroscopic techniques, which have already been applied successfully on [FeFe]-hydrogenases.<sup>21–23</sup> Corresponding experiments to elucidate the structural basis of the catalytic  $\text{Ni}_a\text{-C}$  intermediate and its tautomers  $\text{Ni}_a\text{-L1}$  and  $\text{Ni}_a\text{-L2}$ , which can be easily enriched in the HoxBC complex, are currently underway.

## ■ ASSOCIATED CONTENT

### Supporting Information

The Supporting Information is available free of charge at <https://pubs.acs.org/doi/10.1021/acscatal.0c04079>.

Material and Methods, Supporting Results including molecular biological, spectroscopic and computational data, Tables S1–S3, Figures S1–S12, Supporting References (PDF)

Optimized structures (XYZ format) for all the DFT-computed  $\text{Ni}_a\text{-S}$  models (ZIP)

## ■ AUTHOR INFORMATION

### Corresponding Authors

**Giorgio Caserta** – Institut für Chemie, Technische Universität Berlin, 10623 Berlin, Germany; [orcid.org/0000-0003-0986-3059](https://orcid.org/0000-0003-0986-3059); Email: [giorgio.caserta@tu-berlin.de](mailto:giorgio.caserta@tu-berlin.de)

**Ingo Zebger** – Institut für Chemie, Technische Universität Berlin, 10623 Berlin, Germany; [orcid.org/0000-0002-6354-3585](https://orcid.org/0000-0002-6354-3585); Email: [ingo.zebger@tu-berlin.de](mailto:ingo.zebger@tu-berlin.de)

**Oliver Lenz** – Institut für Chemie, Technische Universität Berlin, 10623 Berlin, Germany; [orcid.org/0000-0003-4550-5128](https://orcid.org/0000-0003-4550-5128); Email: [oliver.lenz@tu-berlin.de](mailto:oliver.lenz@tu-berlin.de)

### Authors

**Christian Lorent** – Institut für Chemie, Technische Universität Berlin, 10623 Berlin, Germany; [orcid.org/0000-0001-9057-4523](https://orcid.org/0000-0001-9057-4523)

**Vladimir Pelmeshikov** – Institut für Chemie, Technische Universität Berlin, 10623 Berlin, Germany; [orcid.org/0000-0002-0523-4418](https://orcid.org/0000-0002-0523-4418)

**Janna Schoknecht** – Institut für Chemie, Technische Universität Berlin, 10623 Berlin, Germany

**Yoshitaka Yoda** – Japan Synchrotron Radiation Research Institute, Hyogo 679-5198, Japan

**Peter Hildebrandt** – Institut für Chemie, Technische Universität Berlin, 10623 Berlin, Germany; [orcid.org/0000-0003-1030-5900](https://orcid.org/0000-0003-1030-5900)

**Stephen P. Cramer** – SETI Institute, Mountain View, California 94043, United States

Complete contact information is available at: <https://pubs.acs.org/doi/10.1021/acscatal.0c04079>

### Author Contributions

G.C. and O.L. conceived and designed experiments. G.C. performed sample preparation, *in vitro* reconstitution, biochemical assays, and IR spectroscopic experiments. C.L. performed and analyzed EPR measurements. G.C., Y.Y. and S.P.C. acquired and analyzed NRVS data. V.P. performed DFT calculations. I.Z. and P.H. contributed to data analysis. O.L. and I.Z. supervised the project. G.C. and O.L. wrote the manuscript with input from all coauthors. All authors have given approval to the final version of the manuscript.

### Notes

The authors declare no competing financial interest.

## ■ ACKNOWLEDGMENTS

G.C., O.L., I.Z., P.H., and S.P.C. are grateful to the Einstein Foundation Berlin (grant number EVF-2016-277) for funding. This work was also supported through the cluster of excellence “UniSysCat” funded by the Deutsche Forschungsgemeinschaft (DFG, German Research Foundation) under Germany’s Excellence Strategy-EXC2008-390540038 and the Einstein

Center of Catalysis (EC<sup>2</sup>)/BIG-NSE. The authors are indebted for EU financial support (Article 38.1.2, GA) within the European Union's Horizon 2020 research and innovation program under grant agreement No 810856. S.P.C. acknowledges funding for his work through NIH GM-65440. NRVS data collection was supported by the [2017B1321, 2019A1201] SPing-8 proposal.

## REFERENCES

- (1) Lubitz, W.; Ogata, H.; Rüdiger, O.; Reijerse, E. Hydrogenases. *Chem. Rev.* **2014**, *114* (8), 4081–4148.
- (2) Shafaat, H. S.; Rüdiger, O.; Ogata, H.; Lubitz, W. [NiFe] Hydrogenases: A Common Active Site for Hydrogen Metabolism under Diverse Conditions. *Biochim. Biophys. Acta, Bioenerg.* **2013**, *1827* (8–9), 986–1002.
- (3) Fritsch, J.; Lenz, O.; Friedrich, B. Structure, Function and Biosynthesis of O<sub>2</sub>-Tolerant Hydrogenases. *Nat. Rev. Microbiol.* **2013**, *11* (2), 106–114.
- (4) Lacasse, M. J.; Zamble, D. B. [NiFe]-Hydrogenase Maturation. *Biochemistry* **2016**, *55* (12), 1689–1701.
- (5) Roncaroli, F.; Bill, E.; Friedrich, B.; Lenz, O.; Lubitz, W.; Pandelia, M.-E. Cofactor Composition and Function of a H<sub>2</sub>-Sensing Regulatory Hydrogenase as Revealed by Mössbauer and EPR Spectroscopy. *Chem. Sci.* **2015**, *6* (8), 4495–4507.
- (6) Horch, M.; Schoknecht, J.; Mroginski, M. A.; Lenz, O.; Hildebrandt, P.; Zebger, I. Resonance Raman Spectroscopy on [NiFe] Hydrogenase Provides Structural Insights into Catalytic Intermediates and Reactions. *J. Am. Chem. Soc.* **2014**, *136* (28), 9870–9873.
- (7) Horch, M.; Schoknecht, J.; Wrathall, S. L. D.; Greetham, G. M.; Lenz, O.; Hunt, N. T. Understanding the Structure and Dynamics of Hydrogenases by Ultrafast and Two-Dimensional Infrared Spectroscopy. *Chem. Sci.* **2019**, *10* (39), 8981–8989.
- (8) Caserta, G.; Lorent, C.; Ciaccafava, A.; Keck, M.; Breglia, R.; Greco, C.; Limberg, C.; Hildebrandt, P.; Cramer, S. P.; Zebger, I.; Lenz, O. The Large Subunit of the Regulatory [NiFe]-Hydrogenase from *Ralstonia eutropha* - A Minimal Hydrogenase? *Chem. Sci.* **2020**, *11*, 5453–5465.
- (9) Ash, P. A.; Liu, J.; Coutard, N.; Heidary, N.; Horch, M.; Gudim, I.; Simler, T.; Zebger, I.; Lenz, O.; Vincent, K. A. Electrochemical and Infrared Spectroscopic Studies Provide Insight into Reactions of the NiFe Regulatory Hydrogenase from *Ralstonia eutropha* with O<sub>2</sub> and CO. *J. Phys. Chem. B* **2015**, *119* (43), 13807–13815.
- (10) Iliina, Y.; Lorent, C.; Katz, S.; Jeoung, J.; Shima, S.; Horch, M.; Zebger, I.; Dobbek, H. X-Ray Crystallography and Vibrational Spectroscopy Reveal the Key Determinants of Biocatalytic Dihydrogen Cycling by [NiFe] Hydrogenases. *Angew. Chem., Int. Ed.* **2019**, *58* (51), 18710–18714.
- (11) Brecht, M.; van Gestel, M.; Buhke, T.; Friedrich, B.; Lubitz, W. Direct Detection of a Hydrogen Ligand in the [NiFe] Center of the Regulatory H<sub>2</sub>-Sensing Hydrogenase from *Ralstonia eutropha* in Its Reduced State by HYSCORE and ENDOR Spectroscopy. *J. Am. Chem. Soc.* **2003**, *125* (43), 13075–13083.
- (12) Tai, H.; Higuchi, Y.; Hirota, S. Comprehensive Reaction Mechanisms at and near the Ni-Fe Active Sites of [NiFe] Hydrogenases. *Dalton Trans.* **2018**, *47* (13), 4408–4423.
- (13) Hidalgo, R.; Ash, P. A.; Healy, A. J.; Vincent, K. A. Infrared Spectroscopy During Electrocatalytic Turnover Reveals the Ni-L Active Site State During H<sub>2</sub> Oxidation by a NiFe Hydrogenase. *Angew. Chem., Int. Ed.* **2015**, *54* (24), 7110–7113.
- (14) Tai, H.; Nishikawa, K.; Suzuki, M.; Higuchi, Y.; Hirota, S. Control of the Transition between Ni-C and Ni-SL<sub>4</sub> States by the Redox State of the Proximal Fe-S Cluster in the Catalytic Cycle of [NiFe] Hydrogenase. *Angew. Chem.* **2014**, *126* (50), 14037–14040.
- (15) Greene, B. L.; Vansuch, G. E.; Chica, B. C.; Adams, M. W. W.; Dyer, R. B. Applications of Photogating and Time Resolved Spectroscopy to Mechanistic Studies of Hydrogenases. *Acc. Chem. Res.* **2017**, *50* (11), 2718–2726.
- (16) Greene, B. L.; Wu, C.-H.; McTernan, P. M.; Adams, M. W. W.; Dyer, R. B. Proton-Coupled Electron Transfer Dynamics in the Catalytic Mechanism of a [NiFe]-Hydrogenase. *J. Am. Chem. Soc.* **2015**, *137* (13), 4558–4566.
- (17) Tai, H.; Nishikawa, K.; Higuchi, Y.; Mao, Z.; Hirota, S. Cysteine SH and Glutamate COOH Contributions to [NiFe] Hydrogenase Proton Transfer Revealed by Highly Sensitive FTIR Spectroscopy. *Angew. Chem., Int. Ed.* **2019**, *58* (38), 13285–13290.
- (18) Kamali, S.; Wang, H.; Mitra, D.; Ogata, H.; Lubitz, W.; Manor, B. C.; Rauchfuss, T. B.; Byrne, D.; Bonnefoy, V.; Jenney, F. E.; Adams, M. W. W.; Yoda, Y.; Alp, E.; Zhao, J.; Cramer, S. P. Observation of the Fe-CN and Fe-CO Vibrations in the Active Site of [NiFe] Hydrogenase by Nuclear Resonance Vibrational Spectroscopy. *Angew. Chem., Int. Ed.* **2013**, *52* (2), 724–728.
- (19) Ogata, H.; Krämer, T.; Wang, H.; Schilter, D.; Pelmeshnikov, V.; van Gestel, M.; Neese, F.; Rauchfuss, T. B.; Gee, L. B.; Scott, A. D.; Yoda, Y.; Tanaka, Y.; Lubitz, W.; Cramer, S. P. Hydride Bridge in [NiFe]-Hydrogenase Observed by Nuclear Resonance Vibrational Spectroscopy. *Nat. Commun.* **2015**, *6*, 7890.
- (20) Caserta, G.; Pelmeshnikov, V.; Lorent, C.; Waffo, A. F. T.; Katz, S.; Lauterbach, L.; Schoknecht, J.; Wang, H.; Yoda, Y.; Tamasaku, K.; Kaupp, M.; Hildebrandt, P.; Lenz, O.; Cramer, S. P.; Zebger, I. Hydroxy-bridged Resting States of [NiFe]-hydrogenase Unraveled by Cryogenic Vibrational Spectroscopy and DFT Computations. *ChemRxiv*. October 15, 2020. DOI: 10.26434/chemrxiv.13079639.v1.
- (21) Gilbert-Wilson, R.; Siebel, J. F.; Adamska-Venkatesh, A.; Pham, C. C.; Reijerse, E.; Wang, H.; Cramer, S. P.; Lubitz, W.; Rauchfuss, T. B. Spectroscopic Investigations of [FeFe] Hydrogenase Maturated with [Fe<sub>2</sub>(Adt)(CN)<sub>2</sub>(CO)<sub>4</sub>]<sup>2-</sup>. *J. Am. Chem. Soc.* **2015**, *137* (28), 8998–9005.
- (22) Pelmeshnikov, V.; Birrell, J. A.; Pham, C. C.; Mishra, N.; Wang, H.; Sommer, C.; Reijerse, E.; Richers, C. P.; Tamasaku, K.; Yoda, Y.; Rauchfuss, T. B.; Lubitz, W.; Cramer, S. P. Reaction Coordinate Leading to H<sub>2</sub> Production in [FeFe]-Hydrogenase Identified by Nuclear Resonance Vibrational Spectroscopy and Density Functional Theory. *J. Am. Chem. Soc.* **2017**, *139* (46), 16894–16902.
- (23) Reijerse, E. J.; Pham, C. C.; Pelmeshnikov, V.; Gilbert-Wilson, R.; Adamska-Venkatesh, A.; Siebel, J. F.; Gee, L. B.; Yoda, Y.; Tamasaku, K.; Lubitz, W.; Rauchfuss, T. B.; Cramer, S. P. Direct Observation of an Iron-Bound Terminal Hydride in [FeFe]-Hydrogenase by Nuclear Resonance Vibrational Spectroscopy. *J. Am. Chem. Soc.* **2017**, *139* (12), 4306–4309.